Solar RRL

WILEY-VCH

Solar RRL

RESEARCH ARTICLE OPEN ACCESS

Development of Boron Emitters for Tunnel Oxide Passivated Contact Solar Cells with Current-Assisted Contact Formation

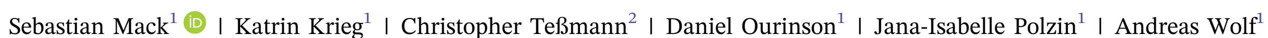

Sebastian Mack[1] | Katrin Krieg[1] | Christopher Teßmann[2] | Daniel Ourinson[1] | Jana-Isabelle Polzin[1] | Andreas Wolf[1]

[1]Fraunhofer ISE, Freiburg, Germany | [2]Fraunhofer Institute for Applied Solid State Physics IAF, Freiburg, Germany

Correspondence: Sebastian Mack (sebastian.mack@ise.fraunhofer.de)

Received: 12 November 2024 | **Revised:** 24 January 2025 | **Accepted:** 29 January 2025

Funding: German Federal Ministry for Economic Affairs and Climate Action via projects “StroKoTOP”, Grant/Award Number: Fkz 03EE1178A; “WamTec”, Grant/Award Number: Fkz 03EE1193; Funding via the Clean Energy Transition Partnership CETP

Keywords: BBr_3 diffusion | emitter | LECO | solar cells | TOPCon

ABSTRACT

Front side recombination in tunnel oxide passivated contact solar cells is frequently described by the recombination parameters j_{0e} for the passivated and $j_{0e,met}$ for the metallized front region. The combination of Al-free metallization pastes and current-assisted contact formation has shown significant reduction of $j_{0e,met}$. Such new metallization approaches enable shallower doping profiles and higher sheet resistances R_{sheet}, which in turn also reduce j_{0e}. In this study, we provide insight into how to reduce the overall front side recombination, by tailoring the boron dopant profile from atmospheric pressure BBr_3 diffusion processes. The limitation of the dopant dose in the profile leads to a higher R_{sheet} of the resulting profile. The newly developed homogeneous boron emitter features $j_{0e} = 14$ fA cm^{-2} at a $R_{sheet} = 161\ \Omega\ sq^{-1}$, a 62% decrease from the initial value, and an even lower $j_{0e} = 8$ fA cm^{-2} is determined for an emitter with $330\ \Omega\ sq^{-1}$. An increased contact resistivity on the front side still poses a challenge for Ag front side pastes despite the use of current-assisted contact formation. Application of an alternative AgAl paste in industrial-type fabricated TOPCon solar cells results in a maximum conversion efficiency of 24.5%.

1 | Introduction

Reducing the overall carrier recombination in silicon-based solar cell concepts is a common approach to improve the conversion efficiency of such devices. Over the last decades, significant changes have been made to the underlying solar cell architectures to reduce carrier recombination at the rear side of the device. Such has been done in the transition from solar cells with Al back surface field to the well-known passivated emitter and rear cell (PERC) by minimizing the area fraction of direct contact between rear metal and Si wafer from roughly 100% to only a few percent. The next evolution step has been the implementation of passivating contacts, such as the tunnel oxide passivated contact (TOPCon) [1] solar cell, which utilizes highly doped silicon layers in combination with an ultrathin tunnel oxide layer [2, 3], to effectively diminish carrier recombination underneath the metal contact. Common to all these solar cells is the use of a diffused junction at the front side of the solar cell, which consists of a silicon region highly doped with a dopant of the opposite doping type than the wafer itself and which requires effective surface passivation by dielectric layers. Typically, contacting such profiles is realized by screen-printed metal pastes and a short contact firing step. Over the years, tremendous improvements have been made especially by metal paste manufacturers, which allowed reducing the necessary dopant concentration in the underlying dopant profiles with each paste generation further and further while maintaining low contact resistivities [4–8]. As lower surface concentrations and lower dopant density in general allow for improved surface

This is an open access article under the terms of the Creative Commons Attribution License, which permits use, distribution and reproduction in any medium, provided the original work is properly cited.

© 2025 The Author(s). *Solar RRL* published by Wiley-VCH GmbH.

passivation and reduced Auger recombination, the front side recombination parameter j_{0e} decreased as well. Nevertheless, recombination at the emitter side dominates the overall recombination in TOPCon solar cells nowadays [9] and therefore lowering this recombination path is an important approach for increasing the conversion efficiency of TOPCon solar cells.

For fabrication of p-type emitters in n-type solar cells, several technologies have been evaluated, such as, for example, high-temperature diffusion processes at atmospheric or low-pressure using BBr_3 [10] or BCl_3 precursors [11], rapid vapor-phase direct doping in H_2/B_2H_6 gas mixtures [12], deposited boron-containing glasses [13] or other layers [14] followed by a drive-in at elevated temperatures, ion implantation [15, 16] and thermal activation, or also screen printing of Al pastes and contact firing [17]. General approaches to reduce recombination in diffused emitters are increasing the emitter sheet resistance [18] (as a result of reduced dopant dose per area unit and thus reduced Auger recombination) or reducing the surface dopant concentration, which reduces surface recombination [19]. Of course, for a fixed sheet resistance or doping dose, also the profile can be tailored, leading to either very shallow profiles with high peak concentration or quite the contrary to deep emitters with low concentration. Also selective boron emitters have received increased attention over the last years [6, 20–23].

The use of an efficient surface passivation is another method to decrease the recombination parameter j_{0e}. Typically, this is realized by the implementation of dielectric layers, which reduce the interface trap density, or comes along with a high fixed charge density, ideally both. For boron emitters, the state-of-the-art passivation layer is a stack of Al_2O_3 and SiN_x, either with or without an ultrathin SiO_x layer between crystalline silicon wafer and the Al_2O_3 layer. Often, atomic layer deposition (ALD) is used as the technology of choice for Al_2O_3 layer deposition [24], but also other technologies such as plasma-enhanced chemical vapor deposition (PECVD) [25] or atmospheric pressure CVD [26] have been evaluated. Among other investigated approaches for boron emitter passivation are stacks of wet chemical or thermal SiO_x and SiN_x dielectrics [27, 28].

Screen printing of Ag-based metallization pastes followed by contact sintering is the dominant metallization technology. Ag pastes are the standard for rear side metallization in TOPCon solar cells with n-doped polysilicon layer, whereas for contacting the boron emitter on the front side, AgAl pastes have been used until recently. A major step for reducing recombination at the front metal contacts has been the introduction of Al-free metallization pastes and current-assisted contact formation [7], as, for example, laser-enhanced contact optimization (LECO) [9, 20, 29–32], which requires the development of suited doping profiles and passivation layers. During LECO, a combination of reverse bias voltage and intense laser illumination leads to microscopic changes at the contact sites, which result in lower contact resistivity on both front and rear [32].

This work reports on the development of boron diffusion processes under atmospheric pressure toward higher sheet resistances, with the goal of reducing the recombination parameter j_{0e}. In addition, we investigate the impact of the process ambient during temperature ramp-down after the drive-in step and how it affects the surface near-doping profile and thereby contact resistivity. Selected processes, that is, for emitter diffusion and passivation, are included into TOPCon solar cell experiments, as apart from recombination properties, also optical properties as well as the compatibility with screen-printed metallization pastes need to be ensured.

2 | Sample Fabrication

2.1 | Symmetric Samples

Symmetric samples are used for determination of the recombination parameter j_{0e}. Sample fabrication begins with alkaline texturing of phosphorus-doped M2-sized Si wafers with a thickness of 180 µm and 1.5 Ω cm resistivity. After cleaning of the wafers, an atmospheric pressure tube furnace process using a BBr_3 liquid precursor forms the boron emitter. Removal of the borosilicate glass layer is the first step for efficient surface passivation, followed by cleaning, both-sided deposition of an Al_2O_3 layer by ALD in single-slot configuration in a tube furnace. A subsequent outgassing step in another tube furnace removes volatile components from the Al_2O_3 layer, which could otherwise lead to blistering. The next step is the deposition of SiN_x layers on front and rear by PECVD. A final short firing step in a conveyor belt improves the passivation properties by hydrogenation of the interface. Quasisteady-state photoconductance (QSSPC) measurements in a Sinton lifetime tester (WCT−120) yield the injection-dependent minority carrier lifetime, typically for three identically processed samples. For extraction of j_{0e}, the measurements are analyzed by application of the slope method [33].

Selected samples are removed from processing after boron diffusion to determine the electrically active dopant profiles by means of electrochemical capacitance voltage (ECV) profiling or the homogeneity of the sheet resistance R_{sheet} by means of four-point probe (4pp) measurements.

2.2 | Solar Cells

For industrial TOPCon (*i*TOPCon) solar cell fabrication, phosphorus-doped M2-sized Cz-Si wafers are used. Processing starts with saw damage removal and random pyramid formation in KOH solution, in separate process baths, differing in concentration and additives. The before-mentioned conventional tube furnace diffusion at atmospheric pressure takes place using a BBr_3 liquid precursor [18]. A diluted HF/HCl solution removes the rear BSG layer in an inline tool, followed by rear emitter removal in KOH solution in a batch system, which in addition ensures an efficient isolation of the wafer edge. Importantly, the front BSG layer needs to be kept intact, thus requiring a certain BSG thickness. The TOPCon interface oxide on the rear side is formed by thermal oxidation. This is followed by deposition of an in situ phosphorous-doped Si layer of around 80 nm thickness by means of PECVD.

Inline wet chemical etching using diluted KOH removes the amorphous Si wrap around at the front side as well as on the edges of the wafers, ensuring a very high shunt resistance and sufficient reverse bias stability. Due to the high selectivity of

2367198x, 2025, 6, Downloaded from https://onlinelibrary.wiley.com/doi/10.1002/solr.202400808 by Fraunhofer Ise Inst. Solar Energy Systems, Wiley Online Library on [24/03/2025]. See the Terms and Conditions (https://onlinelibrary.wiley.com/terms-and-conditions) on Wiley Online Library for rules of use; OA articles are governed by the applicable Creative Commons License

KOH, the front BSG layer is not etched during that process. hydroflouric acid (HF) treatment in the same tool removes the BSG layer, which is followed by wet chemical cleaning of the wafers and thermal annealing for crystallization of the TOPCon layer and achieving a very shallow drive-in of phosphorus through the interfacial oxide into the Si wafer. Our route for passivation consists of ozone cleaning, deposition of an Al_2O_3 layer by ALD in single-slot configuration in a tube furnace (i.e., on both wafer sides), a subsequent outgassing step in another tube furnace, and the deposition of a SiN_x/SiO_xN_y layer stack on the front and a SiN_x layer on the rear by direct-plasma PECVD. Single-step screen printing of a commercial Ag paste on the rear using a 12 busbar (BB) layout and an Ag paste on the front side in a 0BB layout with finger openings of 24 µm in combination with contact firing in an inline conveyor belt furnace form the metal contacts. Finally, the important current–voltage characteristics are extracted in an industrial cell tester, which also includes our LECO unit [32].

Figure 1 shows a schematic of the cross section of the fabricated *i*TOPCon solar cells.

3 | Results and Discussion

3.1 | Tailoring of Boron Dopant Profiles

The sheet resistance R_{sheet} of a doped Si layer is a result of mobility and doping concentration *N*. Typical boron emitter diffusion recipes include a deposition of the dopant source and a drive-in of the dopant at a higher temperature. In-diffusion can be controlled by, for example, changing the dopant concentration of the source, decoupling of source and Si wafer between deposition and drive-in, and different drive-in parameters, such as plateau temperature or duration.

To investigate the effect of different doping profiles on recombination parameters, we vary R_{sheet} from around 120 $\Omega\,sq^{-1}$ initially, denoted with Em0, up to 330 $\Omega\,sq^{-1}$. This was realized by limiting the in-diffusion of dopant by means of the growth of a thermal oxide while leaving the temperature–time profile of the process unchanged. The results of this approach are visible in Figure 2, which shows doping concentration profiles for those processes, extracted from ECV measurements. It is important to mention that the ECV profiles have been scaled to the 4pp measured sheet resistance in the center of the wafer $R_{sheet,center}$.

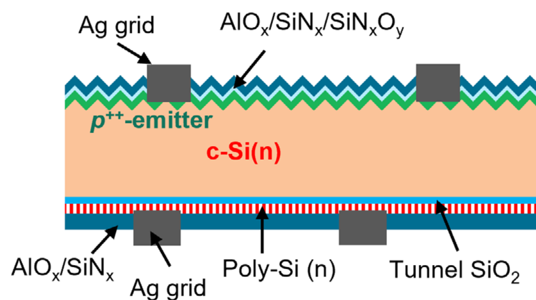

FIGURE 1 | Schematic cross section of the fabricated iTOPCon solar cells.

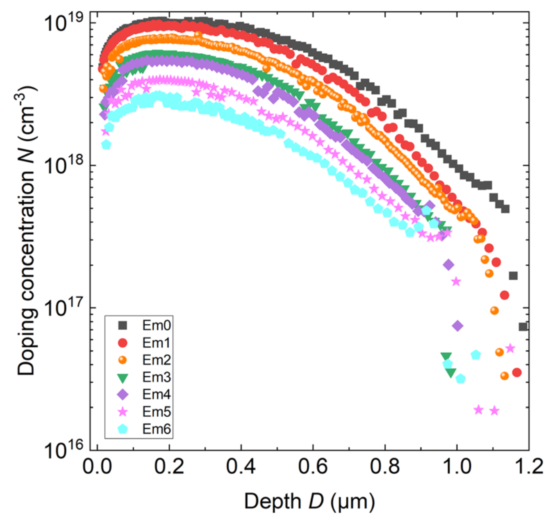

FIGURE 2 | Doping concentration profiles of boron in the emitter determined by ECV, for samples from various BBr_3 diffusion processes. The profiles are scaled to match the locally determined sheet resistance $R_{sheet,center}$. Table 1 lists the characteristics of the different profiles. ECV = electrochemical capacitance voltage.

Table 1 summarizes the characterization results of all diffusions. The variations performed in this survey decrease the total dopant dose per wafer area from initially $Q = 6.6 \times 10^{14}\,cm^{-2}$ down to $Q = 1.5 \times 10^{14}\,cm^{-2}$. Specifically, it results in dopant profiles with both lower surface concentration and reduced depth. The maximum concentration decreases from $N_{max} = 1 \times 10^{19}\,cm^{-3}$ for the reference process Em0 to only $N_{max} = 3 \times 10^{18}\,cm^{-3}$ for process Em6. Similarly, the profile depth *D*, which is determined at a carrier concentration of $1 \times 10^{17}\,cm^{-3}$, decreases from initially around 1.2 µm by roughly 0.2 µm. The surface near region of the profile, described by the surface concentration N_{surf} and the maximum concentration N_{max}, can have a strong impact on the resulting contact resistivity to screen-printed metallization later in the cell process. In addition, junction depth can strongly affect j_{01} and j_{02}-related recombination [34], as well as the blue response, so dopant profiles must not only be optimized only with respect to j_{0e}, but also lateral conductivity, transparency, contact resistivity, and production throughput.

Apart from the local dopant concentration obtained from ECV profiling, the dopant homogeneity over the wafer surface is of utmost importance for solar cells. To determine homogeneity, we apply 4pp measurements, with a 20 × 20 mapping, excluding the corners as well as the center of the wafer, because that position is reserved for ECV measurements. Figure 3 shows the results of a wafer from diffusion process Em2, with an averaged $R_{sheet} = 166.1\,\Omega\,sq^{-1}$, as well as the denoted minimum (Min) and maximum (Max) values. The low standard deviation $\sigma = 5.2\,\Omega\,sq^{-1}$ makes the process compatible for cell processing. As the wafer is placed in diamond-shape orientation within the diffusion tube, one corner of the wafer is located at the highest position. At this position, denoted as "top" in Figure 3, a lower R_{sheet} is determined, which most probably is a result of either locally increased temperature, other gas flow conditions, or a combination of both.

2367198x, 2025, 6, Downloaded from https://onlinelibrary.wiley.com/doi/10.1002/solr.202400808 by Fraunhofer Ise Inst. Solar Energy Systems, Wiley Online Library on [24/03/2025]. See the Terms and Conditions (https://onlinelibrary.wiley.com/terms-and-conditions) on Wiley Online Library for rules of use; OA articles are governed by the applicable Creative Commons License

TABLE 1 | Summary of doping profile characteristics of the tested emitters.

Process	4pp $R_{sheet,mean}$ (Ω sq^{-1})	4pp $R_{sheet,center}$ (Ω sq^{-1})	Total dose Q (10^{14} cm^{-2})	Surface doping concentration N_{surf} (10^{18} cm^{-3})	Maximum doping concentration N_{max} (10^{18} cm^{-3})	Depth D (μm)	Recombination j_{0e} (fA cm^{-2})
Em0	121	118	6.6	4.6	10.3	1.17	21.4
Em1	138	136	5.7	4.8	9.8	1.15	19.2
Em2	166	159	4.4	3.5	8.2	1.10	14.7
Em3	216	203	3.2	3.0	6.1	1.02	12.4
Em4	233	219	2.9	2.3	5.5	1.00	12.8
Em5	290	270	2.0	1.7	4.0	0.98	10.8
Em6	329	330	1.5	1.4	3.1	0.94	10.5

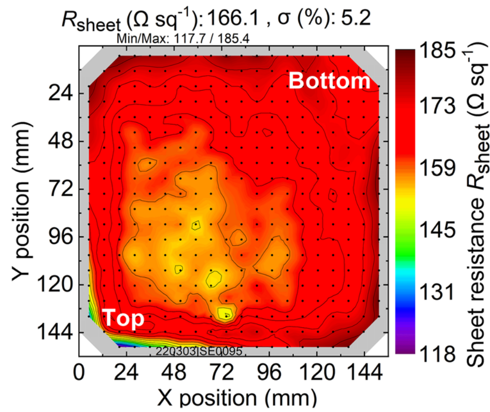

FIGURE 3 | Sheet resistance mapping by 4pp of a wafer after emitter diffusion Em2 and BSG layer removal. BSG = borosilicate glass.

3.2 | Impact of Process Atmosphere During Ramp-Down

As pointed out in Section 3.1, BBr_3 diffusion processes typically consist of two steps, namely, formation of the dopant source and the following drive-in. The first step, formation of the dopant source, controls the homogeneity of the dopant source, and a too short step will result in an inhomogeneous emitter, as will be detectable both over the wafer and also by measuring R_{sheet} along the diffusion boat. The drive-in step is performed at elevated temperature to drive in and redistribute boron within the wafer and thus, affect the emitter depth as well as the maximum and surface dopant concentration. Typically, the drive-in is performed under oxidizing ambient, to prevent boron-rich layer formation [35] and accelerate dopant redistribution by exploiting oxidation-enhanced diffusion. Here, the creation of Si interstitials during thermal oxidation enhances the interstitial-assisted diffusion of boron [36–38]. In addition to this, also the process ambient during ramp-down has an impact on the dopant profile at the surface of the sample, which is especially relevant with respect to contacting.

Figure 4 shows dopant profiles of two emitters, Em2 with an oxygen-containing ambient during ramp-down and emitter Em2N with a ramp-down in nitrogen with the same total gas-flow as Em2. Apart from the ramp-down atmosphere, all other

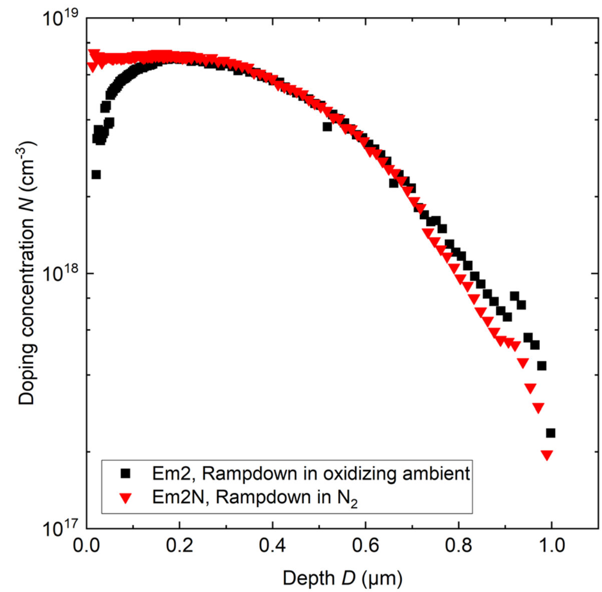

FIGURE 4 | Doping concentration of two boron emitters determined by ECV, with a ramp-down in oxidizing ambient or in nitrogen. The profiles are scaled to match the locally determined sheet resistance $R_{sheet,center}$. ECV = electrochemical capacitance voltage.

process parameters are left unchanged. Em2 features a strong depletion of boron at the surface, with the surface concentration $N_s = 2 \times 10^{18}$ cm^{-3} representing around 30% of the maximum concentration of $N_{max} = 7 \times 10^{18}$ cm^{-3}.

The physical reasons for the depletion at the surface are the higher solubility of boron in SiO_2 compared to Si, as well as the ongoing oxidation of silicon at the interface during ramp-down to doped SiO_2, around twice the thickness of the consumed Si layer, which forms a sink for boron. Also, boron is a slow diffusing impurity in SiO_2 [39]. Here, it is important to remember that the segregation did form already during the drive-in step and continued during ramp-down, but the actual temperature at which this oxidation takes place has also been reported to affect boron depletion at the surface [40]. In contrast to this, the ramp-down in N_2 in process Em2N results in a dopant profile with an almost constant doping concentration within the first 200 nm. The absence of further oxidation after exchange of the process

2367198x, 2025, 6, Downloaded from https://onlinelibrary.wiley.com/doi/10.1002/solr.202400808 by Fraunhofer Ise Inst. Solar Energy Systems, Wiley Online Library on [24/03/2025]. See the Terms and Conditions (https://onlinelibrary.wiley.com/terms-and-conditions) on Wiley Online Library for rules of use; OA articles are governed by the applicable Creative Commons License

ambient leads to a diffusion of boron from the maximum concentration toward the Si/SiO_2 interface, to compensate for local differences in dopant concentration (Fick's first law). According to early studies, the segregation coefficient m is temperature dependent, but as $m < 1$ [41], sometimes $m \approx 0.3$, a diffusion of boron from SiO_2 into Si is less likely. The absence of further oxidation during ramp-down leads to less boron getting consumed in SiO_2, which results in a $9\,\Omega\,sq^{-1}$ lower R_{sheet} for Em2N than Em2. Here, Em2N is characterized by $j_{0e} = 15.8$ fA cm^{-2} at $R_{sheet} = 170\,\Omega\,sq^{-1}$, compared to $j_{0e} = 14.7$ fA cm^{-2} at $R_{sheet} = 179\,\Omega\,sq^{-1}$ for Em2. There is a small difference in R_{sheet} of Em2 compared to the value shown in Table 1, but the diffusions have been performed in different experiments.

3.3 | Emitter Recombination

For solar cells, which will be addressed in the following section, a low j_{0e} is vital for achieving a high V_{oc}. However, j_{0e} needs to be balanced with other loss channels such as lateral resistance from R_{sheet}, and contact resistivity, or metallization-induced recombination. Figure 5 sums up the findings, showing j_{0e} plotted versus $R_{sheet,center}$ for the different emitters (see Table 1) as well as the impact of improved passivation parameters, which have been tested for selected diffusions only. The QSSPC measurements have been performed in the center of three identically processed wafers per group. As a guideline, a restricted in-diffusion of boron and thus lower doping dose leads to a lower j_{0e}. For Em0 and Em2, an optimization of the SiN_x PECVD parameters settings (power, gas flows, times) also allows for slightly reducing j_{0e} at a given $R_{sheet,center}$. For emitter Em0, this results in a 36% decrease of j_{0e} from initially 22 fA cm^{-2} to 14 fA cm^{-2} with the

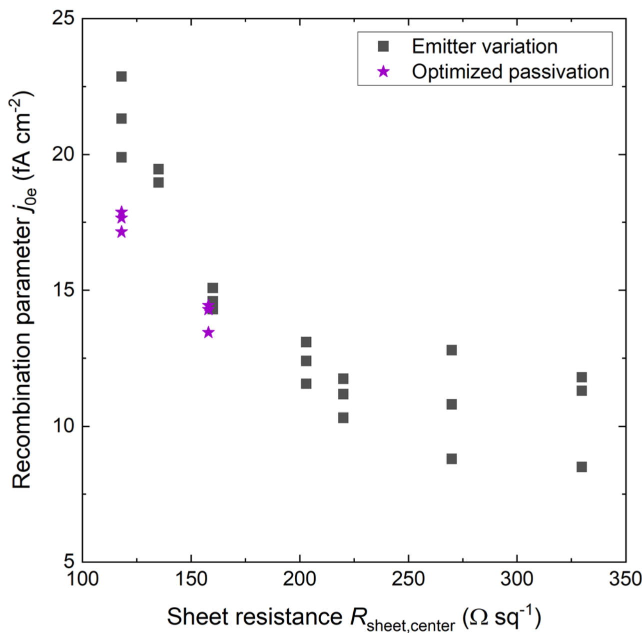

FIGURE 5 | Recombination parameter j_{0e} per side plotted versus sheet resistance $R_{sheet,center}$ and the impact of optimized PECVD passivation. The samples feature a textured surface, passivated by a stack of ALD AlO_x/PECVD SiN_x, and have been measured after hydrogenation in a firing furnace (three samples per process group). ALD = atomic layer deposition; PECVD = plasma-enhanced chemical vapor deposition.

improved PECVD parameters. The lowest $j_{0e} = 8$ fA cm^{-2} is achieved at $R_{sheet,center} = 330\,\Omega\,sq^{-1}$, but also Em4 and Em5 seem to enable $j_{0e} = 10$ fA cm^{-2} as a lower bound, at least for some samples within the groups.

We have also used blue wafers, i.e. solar cells without metallization, to determine the implied open circuit voltage iV_{oc} from QSSPC measurements after a firing furnace step. The results have been published elsewhere [42]. For Em2, an $iV_{oc} = 727$ mV has been reached. A decrease of j_{0e} by changing of the emitter to Em4 has led to $iV_{oc} = 730$ mV, and the implementation of Em6 with a high-quality wafer to an impressive $iV_{oc} = 740$ mV, which indicates the potential for emitters with higher R_{sheet}.

3.4 | Application to Solar Cells

While test structures can help to set up a process or facilitate the extraction of values for simulations, in the end, an optimized process also needs to show an advantage on cell level, which is the ultimate test structure. We selected some promising groups for solar cell fabrication, deciding for emitters Em2, Em4, and Em2 with a cool-down after the drive-in solely in nitrogen, denoted as Em2N. Em0 was ruled out, as in earlier experiments in which we compared Em0 to Em2, solar cells with Em2 showed an advantage of $\Delta\eta = 0.1\%$ absolute.

The solar cell results, which are also denoted *I–V* results as an abbreviation of current–voltage, after LECO treatment, are plotted in Figure 6 versus the contact firing set temperature. It is apparent that a firing set temperature of 790°C is beneficial with respect to solar cell efficiency η, with maximum efficiencies of 24.0% for both Em2 and Em2N, and a standard deviation of below 0.1% for the process groups featuring five to six cells each. As shown above, the ramp-down in N_2 leads to an increase in surface concentration and thus a lower sheet resistance and a higher dopant dose in the emitter. On the one hand, this is expected to result in a slightly higher fill factor (FF) due to higher lateral conductance (<0.1%$_{abs}$ higher FF expected from lower R_{sheet}). On the other hand, the cells with Em2N diffusion exhibit a 1 mV reduced V_{oc} due to higher Auger and increased surface recombination, which is a function of N_{surf} [43, 44]. Both effects level out in terms of efficiency. The median front contact resistivity ρ_c over 132 data points is almost identical with $\rho_c = 3.0$ mΩ cm^2 for Em2 and $\rho_c = 2.9$ mΩ cm^2 for Em2N, as determined from transfer length measurements (TLM). However, solar cells with Em2N feature a 0.2%$_{abs}$ higher pseudo-fill factor (pFF) due to a 0.3 nA/cm^2 lower j_{02}, which is the major cause for the increase in FF compared to Em2 at 790°C firing. Possible reasons for the higher pFF might be a different hydrogenation of both process groups, due to differences in the doping profile or a local accumulation of electrons at the surface. Please note that the solar cells have not been treated by a postfiring illumination or thermal process as published by others [5, 45]. The more pronounced dependance of j_{sc} and V_{oc} on the firing set temperature for Em2N compared to Em2 indicates an interaction of the doping profile with hydrogen passivation.

Solar cells with emitter Em4 and a higher R_{sheet} benefit from less recombination and thus reach a 2 mV higher V_{oc}. However, this group suffers from a reduced FF of only 80%, even after LECO

2367198x, 2025, 6, Downloaded from https://onlinelibrary.wiley.com/doi/10.1002/solr.202400808 by Fraunhofer Ise Inst. Solar Energy Systems, Wiley Online Library on [24/03/2025]. See the Terms and Conditions (https://onlinelibrary.wiley.com/terms-and-conditions) on Wiley Online Library for rules of use; OA articles are governed by the applicable Creative Commons License

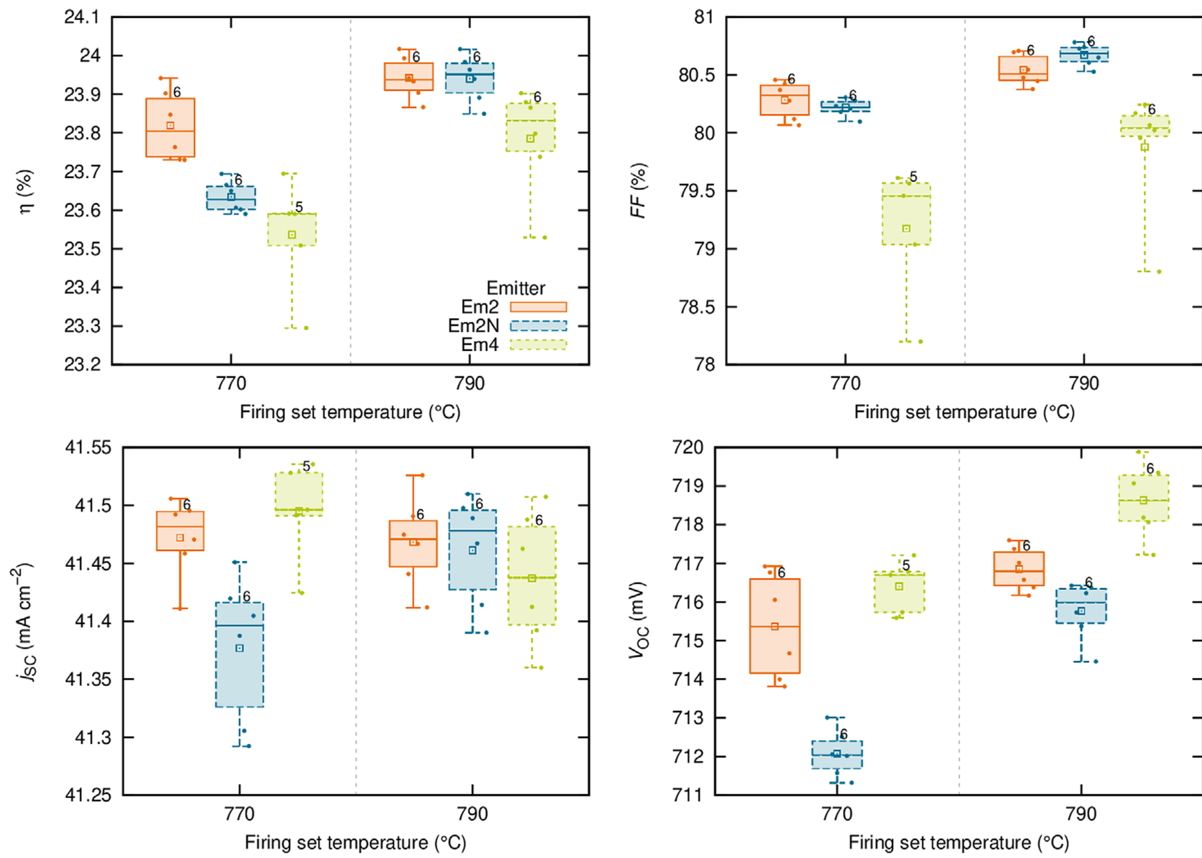

FIGURE 6 | Most important *I–V* data of iTOPCon solar cells measured after LECO treatment at an industrial cell tester for different emitter diffusion recipes and firing set temperatures.

treatment. This trend in FF is even more pronounced when firing at a lower set temperature of 770°C. The reduced FF for Em4 is a result of a higher series resistance of 0.73 Ω cm^2, compared to 0.64 Ω cm^2 for both Em2 groups, at a firing set temperature of 790°C. Apparently, the Ag paste, which is used for contacting of the emitter, struggles with achieving a low ρ_c in case of the Em4 samples.

In terms of j_{sc}, all solar cells are on the same level between 41.4 and 41.5 mA cm^{-2}, only Em2N fired at a set temperature of 770°C yields lower j_{sc} values, as discussed above. In addition, the cells feature a low reverse current density at −12 V $j_{rev,2}$ = 0.1 mA cm^{-2}, which ensures sufficient reverse bias stability for integration of the cells in solar modules.

In order to address the high ρ_c of the Ag paste, we also fabricated solar cells, where we implemented a commercially available AgAl metallization paste on the front side instead of an Ag paste. The results of *I–V* measurement of our champion M2 *i*TOPCon cell featuring emitter Em2 are shown in Table 2, with the measurement being performed at Fraunhofer ISE CalLab PVCells on a reflective chuck, neglecting grid resistance (nomenclature “grn | grn, hrc” [46]). We find a conversion efficiency η = 24.5%, a notable increase toward the results in Figure 6, with a high V_{oc} = 722 mV, j_{sc} = 41.5 mA cm^{-2}, and especially a higher FF of 81.5%. TLM measurements reveal ρ_c = 1.5 Ω cm^2 for the AgAl paste, a reduction to half of the value determined for the Ag paste.

Compared to other published works [6, 20, 22, 31, 47, 48], which partly include selective boron emitters, the main difference lies in FF, which is lower in our case. Thus, future activities will focus on reducing carrier recombination and increasing diode ideality, to boost V_{oc} and pFF, for example, by improved hydrogenation of bulk and interfaces, in addition to other means to increase V_{oc}, for example, by further improvements of emitter passivation, and reducing metallization-related recombination at the front contacts $j_{0e,met}$. Compared to values of others [9, 29], our solar cells with Ag front side paste suffer from a factor of 3 higher contact resistivity on the front side, which needs to be reduced.

TABLE 2 | *I–V* data of our M2-sized champion cell with $AlO_x/SiN_x/SiO_xN_y$ ARC, polysilicon layer deposited by PECVD, and AgAl front side paste. Calibrated measurement at Fraunhofer ISE CalLab PVCells, using a GridTouchTM unit with 30 wires. Measurement on a golden chuck, neglecting grid resistance, nomenclature grn | grn, hrc [46].

Front side paste	Area (cm^2)	η (%)	V_{oc} (mV)	j_{sc} (mA cm^{-2})	FF (%)
AgAl	244.6	24.5	722.2	41.6	81.5

2367198x, 2025, 6, Downloaded from https://onlinelibrary.wiley.com/doi/10.1002/solr.202400808 by Fraunhofer Ise Inst. Solar Energy Systems, Wiley Online Library on [24/03/2025]. See the Terms and Conditions (https://onlinelibrary.wiley.com/terms-and-conditions) on Wiley Online Library for rules of use; OA articles are governed by the applicable Creative Commons License

In other experiments that we conducted, metallization pastes for the front side, which include Al, typically lead to a lower contact resistivity and thus a higher FF, with the drawback of increased $j_{0e,met}$ and thus a lower V_{oc}, compared to pastes without addition of Al components. If ρ_c is on a low level, this points toward the use of Ag pastes in industrial manufacturing to exploit the higher V_{oc}, a step that at least some manufacturers seem to have taken already. Apart from that, the use of Ag pastes has other advantages, such as reducing the need for deep emitters to prevent emitter shunting by the metallization paste, which allows for decreasing diffusion temperatures and process times and positively affecting throughput of diffusion equipment and quartz ware lifetime. Also, recent publications indicate that solar modules with AgAl metallization pastes might be more prone to contact corrosion [30] during damp heat testing. We assume that almost all TOPCon cell manufacturers will choose Ag front side pastes without Al. Recent results in our laboratory also indicate that the combination of a newer Ag front side paste and running LECO with higher power settings (which has been made possible by hardware changes) has led to a lower R_s than it was possible for the experiments described in Sections 3.2 and 3.4.

4 | Summary

This paper highlights the need to reduce the front side recombination parameter j_{0e} by optimization of boron emitter diffusion processes in TOPCon solar cells. This is realized by controlling the total dopant dose in the profile. The optimization described in this paper yields a decrease of j_{0e} by 36% to 14 fA cm^{-2} for process Em2 ($R_{sheet} = 166\,\Omega\,sq^{-1}$) and below 10 fA cm^{-2} for processes with R_{sheet} above 230 $\Omega\,sq^{-1}$. In the TOPCon solar cell, this allows for a certified solar cell efficiency of 24.5% with the developed Em2 process. The potential in V_{oc} and j_{sc} for emitters with $R_{sheet} > 200\,\Omega\,sq^{-1}$ could not yet be fully exploited due to a higher contact resistivity ρ_c at the front side, which leads to a lower conversion efficiency for emitters with high sheet resistance. Future work will address LECO contact formation for improvements in ρ_c.

Another investigation in this paper addresses the impact of the surface near concentration of boron in the emitter. Ramping-down in nitrogen gas instead of an oxygen-containing ambient leads to a flat dopant profile in the first 200 nm in silicon and thus a more than factor 3 increased surface concentration. Besides a slightly reduced V_{oc} due to higher surface and Auger recombination surprisingly, this only marginally affects contact resistivity. Another observed effect is a higher pFF value and a stronger dependance of j_{sc} and V_{oc} on the firing set temperature for the flat profile with higher surface concentration, which indicates an interaction with hydrogen passivation and needs to be investigated in more detail.

Acknowledgments

The authors would like to thank Nico Jung, David Haas, and Mert Isik for excellent processing.

Conflicts of Interest

The authors declare no conflicts of interest.

Data Availability Statement

The authors have nothing to report.

References

1. F. Feldmann, M. Bivour, C. Reichel, H. Steinkemper, M. Hermle, and S. W. Glunz, “Tunnel Oxide Passivated Contacts as an Alternative to Partial Rear Contacts,” *Solar Energy Materials and Solar Cells* 131 (2014): 46–50.

2. E. Yablonovitch, T. Gmitter, R. M. Swanson, and Y. H. Kwark, “A 720 mV Open Circuit Voltage SiOx: C-Si: SiOx Double Heterostructure Solar Cell,” *Applied Physics Letters* 47, no. 11 (1985): 1211–1213.

3. C. Hollemann, F. Haase, S. Schäfer, J. Krügener, R. Brendel, and R. Peibst, “26.1%-Efficient POLO-IBC Cells: Quantification of Electrical and Optical Loss Mechanisms,” *Progress in Photovoltaics: Research and Applications* 26, no. 1 (2019): 3.

4. S. Fritz, S. Riegel, S. Gloger, et al., “Influence of Emitter Properties on Contact Formation to P+ Silicon,” *Energy Procedia* 38 (2013): 720–724.

5. R. Chen, M. Wright, D. Chen, et al., “24.58% Efficient Commercial n-Type Silicon Solar Cells with Hydrogenation,” *Progress in Photovoltaics* 29, no. 11 (2021): 1213–1218.

6. X. Li, Q. Wang, X. Dong, et al., “Optimization of Efficiency Enhancement of TOPCon Cells with Boron Selective Emitter,” *Solar Energy Materials & Solar Cells* 263 (2023): 112585.

7. C. Kim, J.-W. Choi, S. Choi, et al., “Effects of Current-Injection Firing with Ag Paste in a Boron Emitter,” *Scientific Reports* 6, no. 1 (2016): 21553.

8. S. Werner, E. Lohmüller, A. Wolf, et al., “Extending the Limits of Screen-Printed Metallization of Phosphorus- and Boron-Doped Surfaces,” *Solar Energy Materials & Solar Cells* 158 (2016): 37–42.

9. Q. Wang, S. Gu k. Guo, W. Huang, W. Wu, and J. Ding, “Investigation on Effects of the Laser-Enhanced Contact Optimization Process With Ag Paste in a Boron Emitter for n-TOPCon Solar Cell, Prog,” *Progress in Photovoltaics: Research and Applications* 33 (2025): 1–308, https://doi.org/10.1002/pip.3854.

10. E. Lohmüller, M. Glatz, S. Lohmüller, et al., “*BBr3 Diffusion: Process Optimization for High-Quality Emitters with Industrial Cycle Times*,” in 37th European Photovoltaic Solar Energy Conference and Exhibition, WIP Munich, Online 2020, 364–369.

11. R. Monna, V. Sanzone, J. Diaz, and Y. Veschetti, “Influence of the BCl3 Diffusion Process Homogeneity on the Surface Passivation of n-Type PERT Solar Cells,” *Energy Procedia* 92 (2016): 479–485.

12. M. Driesen, A. Richter, J.-I. Polzin, et al., “Simultaneous Boron Emitter Diffusion and Annealing of Tunnel Oxide Passivated Contacts Via Rapid Vapor-Phase Direct Doping,” *IEEE Journal of Photovoltaics* 12, no. 5 (2022): 1142–1148.

13. P. Rothhardt, R. Keding, A. Wolf, and D. Biro, “Co-Diffusion from Solid Sources for Bifacial n-Type Solar Cells,” *Physica Status Solidi (RRL) – Rapid Research Letters* 7, no. 9 (2013): 623–626.

14. J. Seiffe, A. Gahoi, M. Hofmann, J. Rentsch, and R. Preu, “PECVD Al2O3/a-Si: B as a Dopant Source and Surface Passivation: B as a Dopant Source and Surface Passivation,” *Physica Status Solidi A-Applications and Materials Science* 210, no. 8 (2013): 1593–1599.

15. R. Müller, J. Benick, N. Bateman, et al., “Evaluation of Implantation Annealing for Highly-Doped Selective Boron Emitters Suitable for Screen-Printed Contacts,” *Solar Energy Materials & Solar Cells* 120 (2014): 431–435.

2367198x, 2025, 6, Downloaded from https://onlinelibrary.wiley.com/doi/10.1002/solr.202400808 by Fraunhofer Ise Inst. Solar Energy Systems, Wiley Online Library on [24/03/2025]. See the Terms and Conditions (https://onlinelibrary.wiley.com/terms-and-conditions) on Wiley Online Library for rules of use; OA articles are governed by the applicable Creative Commons License

16. J. Krügener, E. Bugiel, R. Peibst, et al., "Structural Analysis of Textured Silicon Surfaces after Ion Implantation under Tilted Angle," *Semiconductor Science and Technology* 29, no. 9 (2014): 95004.

17. C. Schmiga, H. Nagel, and J. Schmidt, "19% Efficientn-Type Czochralski Silicon Solar Cells with Screen-Printed Aluminium-Alloyed Rear Emitter," *Progress in Photovoltaics: Research and Applications* 14, no. 6 (2006): 533–539.

18. S. Werner, E. Lohmüller, U. Belledin, et al., "*Optimization of BBr3 Diffusion Processes for n-Type Silicon Solar Cells*," in 31st European Photovoltaic Solar Energy Conference and Exhibition, WIP Munich, Hamburg 2015, 637–641.

19. A. Kimmerle, M. M. Rahman, S. Werner, et al., "Precise Parameterization of the Recombination Velocity at Passivated Phosphorus Doped Surfaces," *Journal of Applied Physics* 119, no. 2 (2016): 25706.

20. Y. Fan, S. Zou, Y. Zeng, et al., "Investigation of the Ag-Si Contact Characteristics of Boron Emitters for n-Tunnel Oxide-Passivated Contact Solar Cells Metallized by Laser-Assisted Current Injection Treatment," *Solar RRL* 8 (2024): 2400268.

21. Q. Wang, W. Wu, Y. Li, et al., "Impact of Boron Doping on Electrical Performance and Efficiency of n-TOPCon Solar Cell," *Solar Energy* 227 (2021): 273–291.

22. D. Ding, Z. Du, R. Liu, et al., "Laser Doping Selective Emitter with Thin Borosilicate Glass Layer for n-Type TOPCon c-Si Solar Cells," *Solar Energy Materials and Solar Cells* 253 (2023): 112230.

23. W. Lin, D. Chen, C. Liu, et al., "Green-Laser-Doped Selective Emitters with Separate BBr3 Diffusion Processes for High-Efficiency n-Type Silicon Solar Cells," *Solar Energy Materials and Solar Cells* 210 (2020): 110462.

24. G. Dingemans, P. Engelhart, R. Seguin, et al., "Stability of Al_2O_3 and Al_2O_3/a-SiN_x: H Stacks for Surface Passivation of Crystalline Silicon," *Journal of Applied Physics* 106, no. 11 (2009): 114907.

25. P. Saint-Cast, A. Richter, E. Billot, et al., "Very Low Surface Recombination Velocity of Boron Doped Emitter Passivated with Plasma-Enhanced Chemical-Vapor-Deposited AlO_x Layers," *Thin Solid Films* 522 (2012): 336–339.

26. L. E. Black, T. Allen, A. Cuevas, K. R. McIntosh, B. Veith, and J. Schmidt, "Thermal Stability of Silicon Surface Passivation by APCVD Al2O3," *Solar Energy Materials & Solar Cells* 120 (2014): 339–345.

27. H. Ali, A. Moldovan, S. Mack, M. Wilson, W. V. Schoenfeld, and K. O. Davis, "Influence of Surface Preparation and Cleaning on the Passivation of Boron Diffused Silicon Surfaces for High Efficiency Photovoltaics," *Thin Solid Films* 636 (2017): 412–418.

28. V. D. Mihailetchi, Y. Komatsu, and L. J. Geerligs, "Nitric Acid Pretreatment for the Passivation of Boron Emitters for n-Type Base Silicon Solar Cells," *Applied Physics Letters* 92, no. 6 (2008): 63510.

29. A. Mette, S. Hörnlein, F. Stenzel, et al., "Q.ANTUM NEO with LECO Exceeding 25.5% Cell Efficiency," *Solar Energy Materials and Solar Cells* 277 (2024): 113110.

30. X. Wu, X. Wang, W. Yang, et al., "Enhancing the Reliability of TOPCon Technology by Laser-Enhanced Contact Firing," *Solar Energy Materials and Solar Cells* 271 (2024): 112846.

31. C. Guo, R. Jia, X. Li, et al., "Influence of Backside Surface Morphology on Passivation and Contact Characteristics of TOPCON Solar Cells," *Solar Energy* 258 (2023): 278–288.

32. T. Fellmeth, H. Höffler, S. Mack, et al., "Laser-Enhanced Contact Optimization on iTOPCon Solar Cells," *Progress in Photovoltaics: Research and Applications* 30, no. 12 (2022): 1393–1399.

33. D. E. Kane and R. M. Swanson, "*Measurement of the emitter saturation current by a contactless photoconductivity decay method (silicon solar cells)*," 18th IEEE Photovoltaic Specialists Conference (PVSC) (Las Vegas, NV: 1985), 578–583.

34. A. Edler, V. D. Mihailetchi, L. J. Koduvelikulathu, C. Comparotto, R. Kopecek, and R. Harney, "Metallization–induced Recombination Losses of Bifacial Silicon Solar Cells," *Progress in Photovoltaics: Research and Applications* 23, no. 5 (2015): 620–627.

35. M. A. Kessler, T. Ohrdes, B. Wolpensinger, and N.-P. Harder, "Charge Carrier Lifetime Degradation in Cz Silicon through the Formation of a Boron-Rich Layer during BBr3 Diffusion Processes," *Semiconductor Science and Technology* 25, no. 5 (2010): 55001.

36. K. Taniguchi, K. Kurosawa, and M. Kashigawa, "Oxidation Enhanced Diffusion of Boron and Phosphorus in (100) Silicon," *Journal of the Electrochemical Society* 127, no. 10 (1980): 2243–2248.

37. W. Windl, M. M. Bunea, R. Stumpf, S. T. Dunham, and M. P. Masquelier, "First-Principles Study of Boron Diffusion in Silicon," *Physical Review Letters* 83, no. 21 (1999): 4345–4348.

38. A. Ural, P. B. Griffin, and J. D. Plummer, "Fractional Contributions of Microscopic Diffusion Mechanisms for Common Dopants and Self-Diffusion in Silicon," *Journal of Applied Physics* 85, no. 9 (1999): 6440–6446.

39. A. S. Grove, O. Leistiko, and C. T. Sah, "Redistribution of Acceptor and Donor Impurities during Thermal Oxidation of Silicon," *Journal of Applied Physics* 35 (1964): 2695–2701.

40. M. Peng, Q. Wang, M. Zhang, et al., "Optimization of Boron Depletion for Boron-Doped Emitter of N-Type TOPCon Solar Cells," *Materials Science in Semiconductor Processing* 178 (2024): 108424.

41. S. P. Murarka, "Diffusion and Segregation of Ion-Implanted Boron in Silicon in Dry Oxygen Ambients," *Physical Review B* 12, no. 6 (1975): 2502–2519.

42. S. Mack, D. Ourinson, M. Messmer, et al., "Approaches for Reduced Metallization-Induced Losses and Cost in Industrial TOPCon Solar Cells," 42nd EU PVSEC, WIP Munich, Wien 2024, 020041-001–020041-005.

43. B. Hoex, J. Schmidt, R. Bock, P. P. Altermatt, M. C. M. van de Sanden, and W. M. M. Kessels, "Excellent Passivation of Highly Doped p-Type Si Surfaces by the Negative-Charge-Dielectric Al2O3," *Applied Physics Letters* 91, no. 11 (2007): 112107.

44. J. Benick, "*High Efficiency n-Type Solar Cells with a Front Side Boron Emitter*," (Ph.D. thesis, Technische Fakultät, Albert-Ludwigs-Universität, Freiburg im Breisgau, 2010).

45. Z. Hu, L. Song, D. Lin, et al., "Carrier Injection and Annealing-Enhanced Electrical Performance in Tunnel Oxide-Passivated Contact Silicon Solar Cells," *Physica Status Solidi A-Applications and Materials Science* 219 (2022): 2100614.

46. M. Rauer, A. Fell, W. Wöhler, et al., "The Impact of Measurement Conditions on Solar Cell Efficiency," *Solar RRL* 8, no. 3 (2024).

47. Q. Wang, L. Yuan k. Guo, L. Li, et al., "Boron Tube Diffusion Process Parameters for High-Efficiency n-TOPCon Solar Cells with Selective Boron Emitters," *Solar Energy Materials and Solar Cells* 253 (2023): 112231.

48. W. Chen, X. Liu, W. Liu, Y. Yu, W. Wang, and Y. Wan, "Optimization of Activated Phosphorus Concentration in Recrystallized Polysilicon Layers for the n-TOPCon Solar Cell Application," *Solar Energy Materials & Solar Cells* 252 (2023): 112206.

2367198x, 2025, 6, Downloaded from https://onlinelibrary.wiley.com/doi/10.1002/solr.202400808 by Fraunhofer Ise Inst. Solar Energy Systems, Wiley Online Library on [24/03/2025]. See the Terms and Conditions (https://onlinelibrary.wiley.com/terms-and-conditions) on Wiley Online Library for rules of use; OA articles are governed by the applicable Creative Commons License